5G SIW-Based Phased Antenna Array With Cosecant-Squared Shaped Pattern

Jan Puskely, Tomas Mikulasek, Yanki Aslan, *Member, IEEE*, Antoine Roederer, *Life Fellow, IEEE*, and Alexander Yarovoy, *Fellow, IEEE*

***Abstract*— In this article, a concept of a phased antenna array based on substrate integrated waveguide (SIW) technology for 5G base stations is proposed. The array has a cosecant radiation pattern in the vertical plane for uniform illumination in a sector area. The array itself consists of 16 SIW traveling wave subarrays of 12 slot-coupled microstrip patch antennas associated with a pair of reflection-canceling vias and phasing elements to get the tapered distribution both in amplitude and phase for the cosecant-shaped radiation pattern. The array is designed to be operational at 28 GHz with a bandwidth of more than 10%, a candidate mm-wave frequency band for 5G. The phased antenna array supports wide-angle scanning of +/−60° in azimuth and exhibits good active impedance properties. The array design is successfully verified experimentally.**

***Index Terms*— 5G base station, cosecant-squared radiation pattern, microstrip patch antenna, phased antenna array, substrate integrated waveguide (SIW).**

I. Introduction

THE ambitious requirements of 5G systems on the channel capacity, link quality, cost, and reliability demand novel antenna design solutions at millimeter waves. In particular, 5G base station antennas are expected to provide multiple simultaneous beams using the same frequency (sub)band with limited interference, suitable processing complexity, acceptable power consumption, and simple thermal management [1].

Potential true multibeam generation strategies as presented in the 5G literature consider digital, analog, and hybrid architectures [2], [3].

Most of the proposed array topologies consist of square 8 × 8 or 16 × 16 arrays of microstrip patches with square lattices and half-wavelength element separation. Massive MIMO "beam" forming is used both in azimuth and elevation in order to reuse the same subbands at a maximum number of users, with maximum gain and minimum co-channel interference.

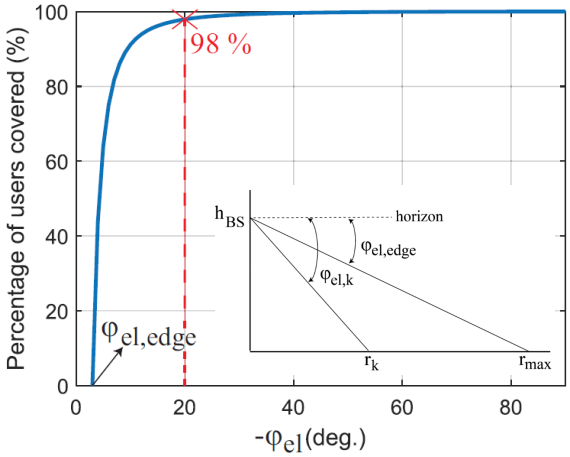

Fig. 1. Percentage of user coverage with respect to $\varphi_{el,k}$ in a cell with uniformly distributed users over the area for $h_{BS} = 10.5$ m and $r_{max} = 200$ m [5].

This results in massive complexity, power consumption, and heat generation, particularly if full digital beam forming is used. Then, one complex weight per element and per user stream must be computed and applied using one two-way baseband to RF digital to analog chain per element.

Such designs are not optimally suited for most 5G base station antennas typically looking down from a 10.5 m street light pole at a +/−60° angular sector of 200 m radius or more [4]. For such base stations, as shown in Fig. 1, around 98% of ground level users are normally within an angle of 20° from the light pole horizon. Using the proposed arrays, with beamwidths of 14° (8 × 8) or 7° (16 × 16), there is clearly little scope for frequency reuse in elevation.

To reduce the processing and hardware complexity, hybrid analog–digital beam forming approaches have been proposed. The idea of hybrid beamforming was first applied for radar phased array antennas [6]. Single-port subarrays of analog phased elements are fed by digitally weighted and time delayed signals. This reduces the number of D/A and A/D as well as up and down frequency conversion chains.

Hybrid beam forming is currently considered by many as the most suitable candidate for 5G base stations at millimeter waves [7], [8]. In the case of an array antenna

Manuscript received September 18, 2020; revised February 24, 2021; accepted May 30, 2021. Date of publication July 26, 2021; date of current version January 11, 2022. This work was supported in part by the Dutch Research Council (NWO) and in part by NXP Semiconductors in the Framework of the Program on Advanced 5G Solutions-Antenna Topologies and Front-End Configurations for Multiple Beam Generation (www.nwo.nl). *(Corresponding author: Jan Puskely.)*

Jan Puskely, Yanki Aslan, Antoine Roederer, and Alexander Yarovoy are with the Department of Microelectronics, Microwave Sensing, Signals and Systems Group, Delft University of Technology, 2600 GA Delft, The Netherlands (e-mail: J.Puskely-1@tudelft.nl; Y.Aslan@tudelft.nl; A.G.Roederer@tudelft.nl; A.Yarovoyg@tudelft.nl).

Tomas Mikulasek is with the Department of Radio Electronics, Brno University of Technology, 61200 Brno, Czech Republic (e-mail: mikulasekt@feec.vutbr.cz).

Color versions of one or more figures in this article are available at https://doi.org/10.1109/TAP.2021.3098577.

Digital Object Identifier 10.1109/TAP.2021.3098577

with multiple simultaneous beam/streams, there are two basic options.

1) Subconnected hybrid beam forming configurations [7].
2) Fully connected configurations [7].

There are some drawbacks of these topologies such as the limited scope of elevation beam scanning, the poor equivalent isotropically radiated power (EIRP) and resolution performance of option 1), and the high and costly combining losses of option 2). It leads naturally to study a third option of hybrid beam forming.

An effective and well-known (in radar) approach in hybrid beam forming is to form a single analog beam in the elevation plane with a cosecant-squared shape and digitally control the beams in the azimuth plane. Besides decreasing the cost and complexity significantly, the cosecant-squared shape in elevation is particularly suited for 5G base stations since.

1) The power flux is equalized for users at different ranges which provides more predictable minimum SNR.
2) Overshadowing of weak signals by the stronger ones near the base station is prevented (crucial for additional code division multiple access (CDMA) [9]).
3) Safety issues related to the vertical compliance distance are automatically resolved [10].
4) Inefficient additional base station user power control is avoided.

Moreover, the competitive statistical performance of the cosecant-squared-based approach in terms of user signal-to-interference-plus-noise ratios (SINRs) was proven in [11] using a multiuser 5G system model.

A wide range of antennas have been proposed for the realization of cosecant-squared pattern. Among them, reflector antennas can yield a high gain and broad bandwidth, but they are large in size, heavy, and costly to fabricate [12], [13]. Reflect arrays need feeding horns with high precision and can only provide one azimuth beam at a time [14], [15]. On the other hand, planar microstrip array antennas can result in a lightweight and low-profile product [16], [17]. However, microstrip-line feeding causes parasitic radiation and large losses, especially at high frequencies [18]. To improve the efficiency of the feeding network, the substrate integrated waveguide (SIW) technique with low cost and high integration capability is commonly adopted [19]–[24]. The introduction of cosecant-based hybrid beam forming in millimeter wave, multiuser 5G applications was first presented in [25] using an antenna system based on longitudinal slots fed by SIW in combination with microstrip patches. Such an antenna structure realizes the horizontal (transverse to the waveguide axis) polarization of transmit waves.

In this article, we propose to combine the transversal slots for vertical (along the waveguide axis) polarization with a microstrip patch to achieve higher gain (allowing for the required +55 dBm EIRP) and much wider operational bandwidth in comparison with previous author's work [24]. Pair of reflection-canceling vias and a phase element are added to SIW to realize a tapered distribution both in amplitude and phase and provide a cosecant shaped radiation pattern. This novel aperture coupled microstrip patch antenna (AC-MPA) array concept can be used in any SIW series-fed array realizing any amplitude and phase distribution along the line and is an attractive alternative to reflection-canceling slot pairs [21]. In this article, the concept is realized for the frequency band 27.5–29.5 GHz, targeting the mm-wave subband for 5G systems.

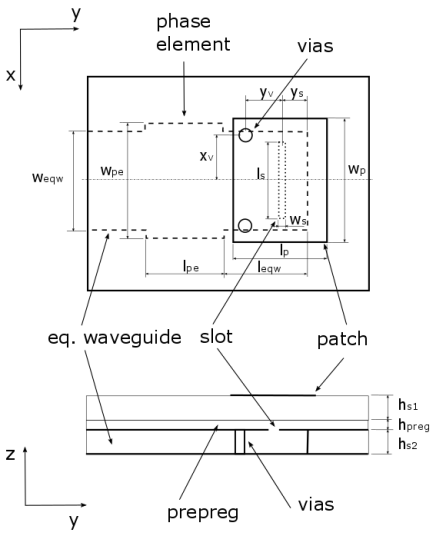

Fig. 2. Geometry of the last element of SIW-fed AC-MPA.

The rest of this article is organized as follows. The basic antenna structure and the design procedure of the slot array with a cosecant radiation pattern are described in Section II. Section III is dedicated to the comparison of the different antenna topologies/strategies for azimuthal scanning phased antenna array. Experimental verification of the cosecant phased antenna array is demonstrated in Section IV. Comparison with traditional concept and discussion are in Sections V and VI, respectively.

II. Design of a Phased Antenna Array With Cosecant-Squared Shaped Radiation Pattern

The cosecant-squared shaped pattern requires a nonuniform amplitude and phase distribution along the waveguide axis. This is why the basic series-fed subarray should allow to control both amplitude and phase.

A. AC-MPA SIW Element of Cosecant Subarray

The transverse slot complemented by a pair of reflection-canceling vias and a phase shifter [24] is a good starting point for the SIW-based array with an arbitrary amplitude and phase distribution along the line due to the independent control of the amplitude and phase distributions. To overcome the limitations of a transverse slot in terms of impedance bandwidth (which is only about 3%) and gain, another dielectric layer with a microstrip patch on the top is added.

The final antenna element, depicted in Fig. 2, consists of three dielectric layers: an SIW feeding layer, a patch layer, and a prepreg layer between them. The rectangular microstrip patch is placed on the top surface of the patch layer with relative permittivity of 2.2 (RT5880) and a thickness h_{s1}. The microstrip patch is aperture coupled through the transversal

TABLE I
DIMENSIONS OF THE ANTENNA IN FIGS. 3 AND 4

Parameters	Value [mm]	Parameters	Value [mm]
l_{pe}	3.000	l_{sp}	6.799
l_{eqw}	5.299	d_{via}	0.300
w_{eqw}	2.866	h_{s1}	0.508
y_s	3.399	h_{s2}	0.635
w_p	3.500	h_{preg}	0.096
w_s	0.200		

slot integrated to the SIW feeding layer with a relative permittivity of 6.15 (RO3006) and a thickness h_{s2}. The slot and the pair vias of the last element are placed in such way to minimize the reflection from the waveguide termination. The patch is placed symmetrically to the center of the slot. The position of reflection-canceling vias, the phase element size, and the patch and slot size are used as tuning parameters in the final cosecant-squared subarray design. FastRise27, with permittivity 2.7, is used as a prepreg layer. To simplify the antenna model, the SIW is substituted by an equivalent rectangular waveguide (WG) of width w_{eqw} [26]. The dimensions of the element in Fig. 2 are listed in Table I.

By numerical analysis of a single radiating element without the phase shifter [Fig. 3(a)], the design curves were derived and depicted in Fig. 3(b). The coupling coefficient decreases with the patch length l_p, while the positions x_v and y_v of the reflection-canceling vias change to minimize the reflection from the element. The phase delay increases with coupling coefficient and has to be taken into account for the desired phase distribution. The design curves are valid for the given relative permittivity of the substrate and the width of the feeding waveguide w_{eqw}.

The uniformly spaced subarray with an amplitude and phase distribution, which realizes cosecant-squared shaped radiation pattern, combines 12 of such radiating elements (Fig. 4). The number of elements is a trade-off between gain and subarray dimension [25]. We can somewhat better approximate the shape of the realized cosecant-squared radiation pattern with a higher number of elements but the gain, limited by the directivity associated with the cosecant-squared template, does not increase significantly. The spacing among the elements is $0.65\lambda_0$ at the operating frequency of 28.5 GHz.

The subarray design consists of two steps: determining excitation coefficients (cosecant beam synthesis) and its realization through amplitude and phase controlling elements.

B. Cosecant-Shaped Beam Synthesis

In the first step, the excitation coefficient of each element was determined. Many algorithms to synthesize cosecant-squared shaped array factors exist in the literature [27]–[33]. To reach the required cosecant-squared radiation pattern, a tapered amplitude and a phase distribution were synthesized by an in-house developed iterative power synthesis technique. Starting from the real wanted cosecant amplitude pattern template, the phase law assigned to the amplitude template is iteratively replaced by that obtained for the realized pattern in the previous iteration. The new complex wanted pattern is then

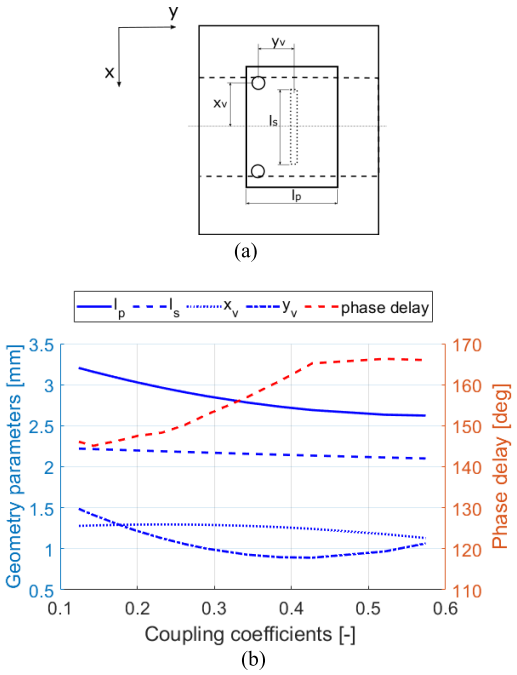

Fig. 3. Configuration of (a) proposed basic antenna element and (b) geometry parameters and phase delay of antenna element against coupling coefficient at 28.5 GHz.

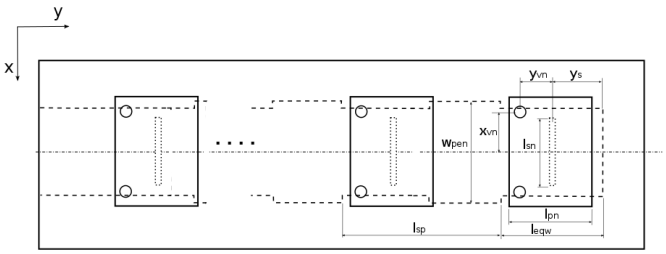

Fig. 4. Cosecant-squared linear subarray of 12 AC-MPA elements fed by an SIW.

projected on the subspace of the array's realizable patterns. Convergence is easy to demonstrate and related to the number of array elements.

The template shown in Fig. 5 was taken as an ideal one in the synthesis process. The final excitation coefficients for the subarray are depicted in Fig. 5. The cosecant-squared radiation pattern related to the given excitation coefficients is also shown in Fig. 5.

C. Design of an AC-MPA Subarray With Cosecant-Squared Radiation Pattern

The amplitude distribution determines the coupling coefficients of the transverse slots and patches based on [16]

$$C(n) = \frac{|A(n)|^2}{\sum_{i=n}^{N} |A(i)|^2} \tag{1}$$

where $A(n)$ is the excitation coefficient of nth element. The coupling coefficient of nth element $C(n)$ represents a ratio of the radiated power P_{rad} to the input power P_{in} and is expressed

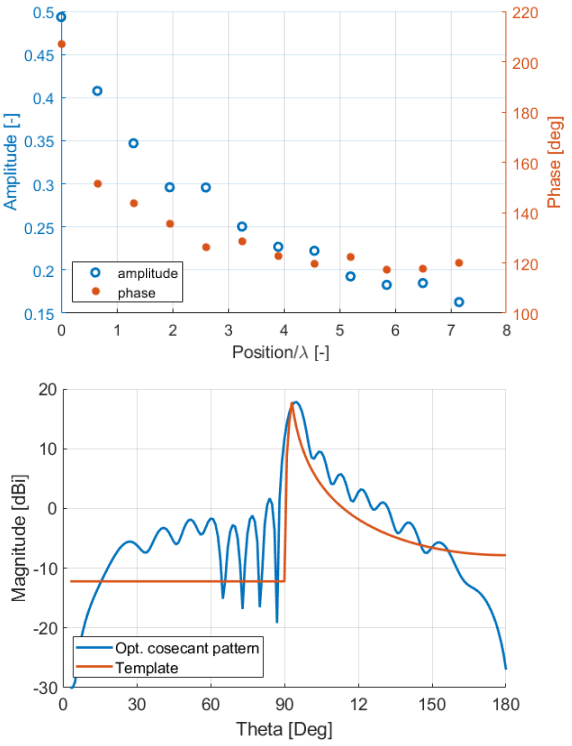

Fig. 5. Excitation coefficients for the 12-element subarray with cosecant-squared shaped beam (top) and corresponding radiation pattern with ideal template (bottom).

TABLE II
GEOMETRY PARAMETERS OF SUBARRAY ELEMENTS IN mm

el. number	l_p	l_s	w_{pe}	x_v	y_v
1	2.906	2.135	2.866	1.287	0.859
2	2.915	2.431	3.295	1.285	0.749
3	2.879	2.724	2.571	1.316	0.596
4	2.994	2.336	2.547	1.277	1.238
5	2.926	2.257	2.574	1.295	0.997
6	2.933	2.401	2.497	1.265	1.149
7	2.931	2.211	2.547	1.278	1.104
8	2.857	2.259	2.561	1.258	0.869
9	2.857	2.199	2.517	1.249	1.001
10	2.809	2.099	2.597	1.216	0.895
11	2.657	2.170	2.687	1.096	0.922
12	2.574	2.472	2.352	no vias	

in terms of scattering parameters as

$$C(n) = \frac{P_{rad}}{P_{in}} = \frac{1 - |s11|^2 - |s21|^2}{1 - |s11|^2}. \quad (2)$$

The coupling coefficient is changed mainly with the patch length l_p. Nevertheless, the slot length l_s and the positions x_v and y_v of the reflection-canceling vias have also an effect on the coupling coefficient. The final dimensions of elements in Table II differ slightly in comparison with design curves in Fig. 3 due to fine optimization of antenna element including the phase shifter.

The phase of the traveling wave between adjacent antenna elements is controlled by the phase element (Fig. 2) represented by the parameters ($l_{\rm pe}$, $w_{\rm pe}$). The targeted phase

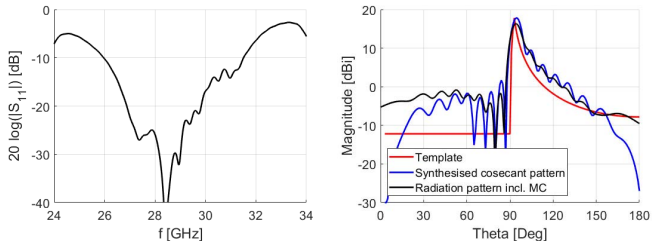

Fig. 6. AC-MPA subarray results. Left: Reflection coefficient. Right: Radiation patterns at 28.5 GHz.

delay is achieved by changing only the parameter $w_{\rm pe}$ of the phase element. The wider SIW leads to a smaller propagation constant and a higher phase shift. So the transverse slot controls the amount of the radiation power, while the phase shifter controls the phase of the transmitted wave.

In the fine optimization process, mutual coupling (MC) among the elements was included by taking into account one adjacent element on each side. The optimized dimensions of the subarray are listed in Table II.

The simulated results of the cosecant linear SIW-fed AC-MPA subarray are shown in Fig. 6. The simulated reflection coefficient indicates an impedance bandwidth of about 20%. The radiation pattern in the vertical plane has a maximum gain of 16.3 dBi which is of about 1.5 dB lower than for synthesized pattern based on isolated radiating elements due to MC among elements.

III. COMPARISON OF DIFFERENT ANTENNA TOPOLOGIES, REGULAR VERSUS IRREGULAR

In high-capacity multiuser applications with multiple users sharing the same time–frequency-code resources, it is crucial to sufficiently suppress the interference among the users. In line of site (LoS)-dominated environments as in the mm-wave 5G networks [34], under a low-complexity beam steering-based precoding, there is a direct relation between the average side lobe level (SLL) radiated by the base station and the statistical quality-of-service (QoS) [4]. For a dense and regularly ($0.5\lambda_0$) spaced array, the high first SLL (that is around -13 dB) becomes responsible for the performance degradation. A power efficient and practical way to lower the peak SLL (for multiple steerable beams inside the sector) is to optimize the positions of the array elements (subarrays) [35]. Yet, applying such density-tapering techniques leads to an increased field strength at the far sidelobes so as to compensate the lower first sidelobe(s). Therefore, the peak SLL in the position-optimized arrays should be made low enough to satisfy the required QoS [11].

In order to investigate the extent of SLL reduction with irregularly spaced cosecant subarrays, we have performed a study with subarray position optimization in different study cases in terms of the number of subarrays and the angular width of the sector in azimuth. The findings on the peak SLL with respect to the corresponding array's broadside beam and the average subarray spacings are reported in Table III. The intersubarray spacing and radiation patterns of two cases from Table III are shown in Fig. 7 as an example. The results are

TABLE III

MAXIMAL FIELD STRENGTH WITH RESPECT TO THE CORRESPONDING BEAM AT BROADSIDE AND AVERAGE INTERSUBARRAY SPACING AFTER THE SUBARRAY POSITION OPTIMIZATION USING THE TECHNIQUE IN [34]

Number of sub-arrays	Sector width in azimuth	+/- 30º	+/- 45º	+/- 60º
16	Peak SLL	-18.4 dB	-17.0 dB	*NA
	Avg. subarray spacing	0.60λ	0.58λ	*NA
24	Peak SLL	-19.9 dB	-18.9 dB	-14.6 dB
	Avg. subarray spacing	0.61λ	0.62λ	0.70λ
32	Peak SLL	-21.2 dB	-19.7 dB	-15.6 dB
	Avg. subarray spacing	0.61λ	0.60λ	0.85λ
48	Peak SLL	-22.9 dB	-22.1 dB	-16.8 dB
	Avg. subarray spacing	0.64λ	0.62λ	0.99λ

*NA: No advantage in SLL reduction as compared to the reference uniformly-(0.5λ) spaced array of subarrays which yields -13.2 dB peak SLL.

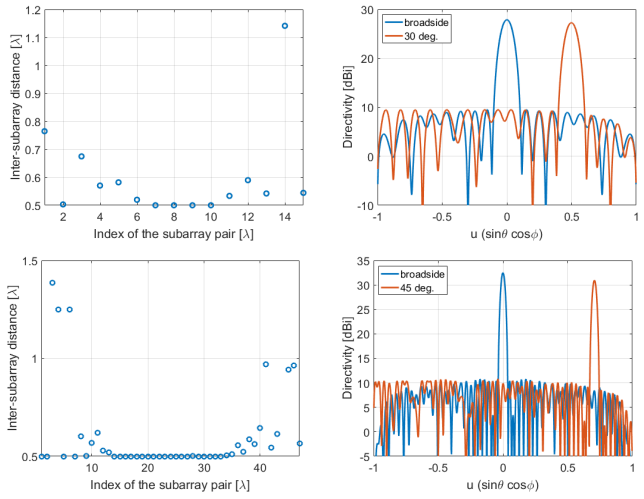

Fig. 7. Intersubarray spacing and radiation patterns of two cases from Table III. Top: 16 subarrays, +/−30° sector. Bottom: 48 subarrays, +/−45° sector.

based on the radiation pattern of the designed cosecant-squared subarray from Section II.

In our application, as we would like to minimize the number of array panels and achieve good statistical QoS, we aim to design an array that is operational in +/−60° scanning range and has SLL below −20 dB and gain more than 25 dBi. In such a wide-angle scanning scenario, 1-D position-only tapering does not bring a significant advantage in peak SLL suppression, as shown in Table III, unless the array is made very large.

Since we want to keep the design, fabrication, and calibration complexity/cost low and also because the abovementioned antenna requirements are fulfilled, we have prototyped a 16-element regularly ($0.5\lambda_0$) spaced array of active subarrays and exploited the capabilities of the beamforming chips.

In the presented prototype, potentially, the required SLL can be achieved via programming of the chips for standard

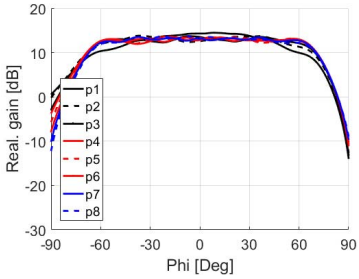

Fig. 8. Computed embedded radiation patterns of eight subarrays; p1 is outer subarray and p8 is in the middle one.

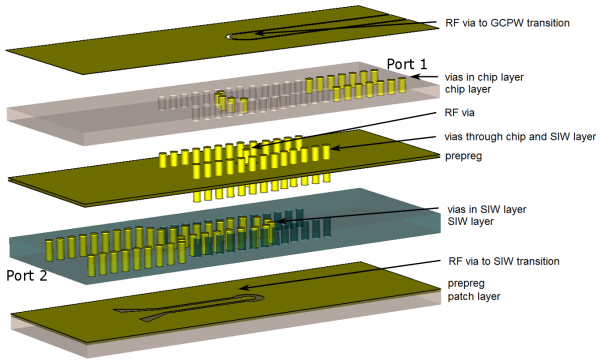

Fig. 9. Two-layer SIW transition between the SIW feeding layer and the chip layer.

amplitude tapering, phase optimization [36], or amplitude and phase optimization [37], at the expense of a reduced power efficiency as compared with the regular or position-optimized arrays.

The whole array consists of "only" 16 half-wavelength spaced subarrays. There was no need for dummy elements on both sides because the embedded radiation patterns of all active subarrays are similar, as shown in Fig. 8.

It is worth to mention that the 3 dB beamwidth of embedded patterns is of about 150°. Despite lower coupling between the subarrays, there is still the parasitic radiation by mainly the first neighbor subarrays which contributes to the embedded radiation pattern. Another factor which contributes to the shape of the radiation pattern and makes it flat is the size of the ground plane.

Since the cosecant-squared subarrays are a part of the active phased array antenna, the PCB layout has to be complemented with another layer which will support K_a-band analog beam forming chips and create also symmetrical stack-up for the physical realization. We designed a two-layer SIW transition between the SIW feeding layer and the new added chip layer for this purpose (see Fig. 9). The transition avoids the leakage in the prepreg layer and its insertion loss is lower than 0.5 dB, as shown in Fig. 10.

The calculated results, such as active reflection coefficients and scan radiation patterns, are presented in Section IV.

IV. REALIZATION AND MEASURED RESULTS

In the final realization, the equivalent rectangular WG is replaced by an SIW using the procedure described in [26]. The phased array antenna was fabricated with a standard

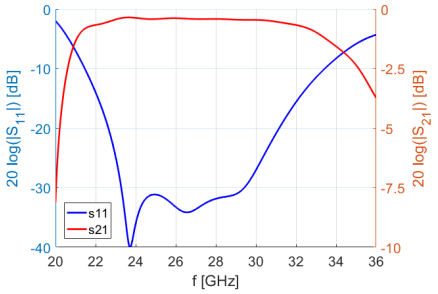

Fig. 10. S-parameters of transition from Fig. 9.

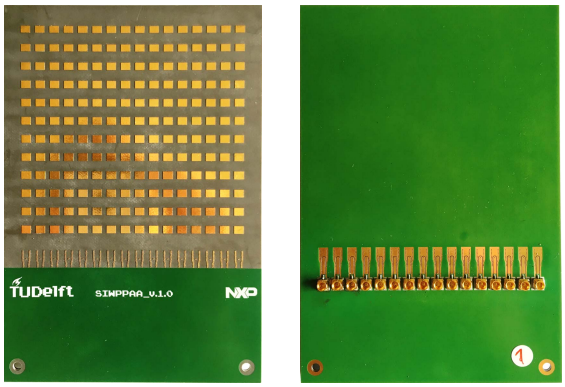

Fig. 11. Fabricated 1 × 16 cosecant-squared phased antenna array.

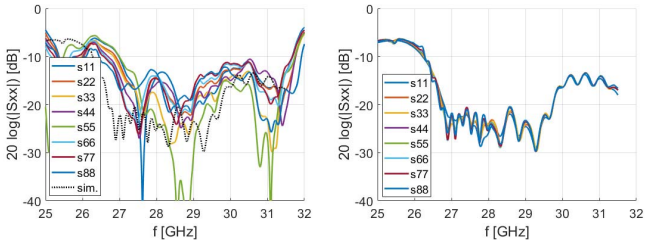

Fig. 12. Reflection coefficient of the AC-MPA subarrays. Left: Measurement. Right: Simulation.

printed circuit board process. The total dimensions of the array are 97 mm × 141 mm. To verify the properties of the antenna array, the array was fabricated and each subarray was equipped with sub miniature push-on mini (SMPM) surface mount connectors, as shown in Fig. 11.

A. Impedance Properties of the Phased Array Antenna

The measured and calculated reflection coefficients at eight input ports are shown in Fig. 12. Port 1 is on the left side and port 8 in the middle in Fig. 11. The calculated results do not take into account the effect of the SMPM connectors. The reflection coefficient of the connectors is better than −15 dB in the given frequency band. Despite the influence of the connectors themselves and the quality of the assembly process on the final results, the measured impedance bandwidth is still more than sufficient for the considered application.

We also analyzed the MC between the subarrays (see Fig. 13). MC below −20 dB has been achieved in both,

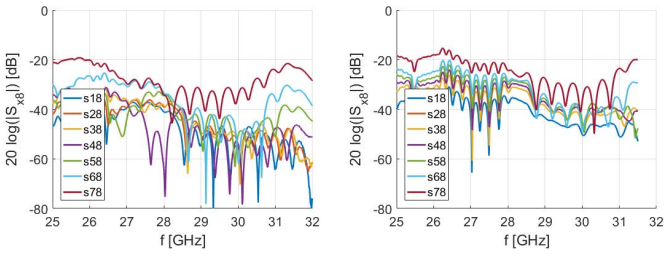

Fig. 13. MC between the subarrays. Left: Measurement. Right: Simulation.

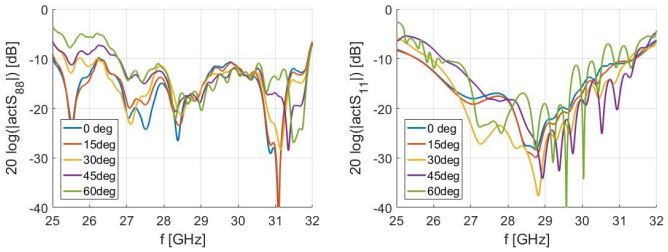

Fig. 14. Active reflection coefficient. Left: Measured port 8. Right: Simulated infinite antenna array.

the simulation and the measurement, in the frequency band 27–31 GHz. The low coupling is due to orientation of slots. It gives us a good premise for the wide range scanning.

The active reflection coefficient as a function of the scan angle in the azimuthal plane is shown in Fig. 14. The calculated active reflection coefficients are valid for the infinite array in the azimuthal plane; the measured ones for the central port 8. The scanning performance is maintained for scan angles up to ±60°. The measured results correspond to those of the infinite array in terms of operational bandwidth which is about 18% (27–32 GHz) in the scanning range of ±60°.

B. Radiation Properties of the Cosecant-Squared Phased Array Antenna

The scan radiation patterns are based on measurement of the embedded patterns of each subarray and subsequent post-processing.

The measured vertical cuts of the embedded patterns and their comparison with the simulated ones (realized gain) in the desired frequency range 28–29 GHz are shown in Fig. 15. One can observe good agreement with simulations in terms of the radiation pattern shape and realized gain which was between 14.3 dBi (at 28 GHz) and 14.8 dBi (at 29 GHz). The cross-polarization patterns in the given cut are shown in Fig. 15 as well, with levels lower than −30 dB in the range ±90°.

The combined radiation patterns of the cosecant phased array antenna based on measured embedded patterns are shown in Figs. 16 and 17. The measured and simulated radiation pattern in a vertical cut at 28.5 GHz is shown in Fig. 16. Good agreement with a cosecant-squared shaped pattern is obtained below horizon. Some pattern degradation takes place above the horizon in terms of the SLL. At the frequency of 28.5 GHz, the main lobe is directed to 4° below horizon.

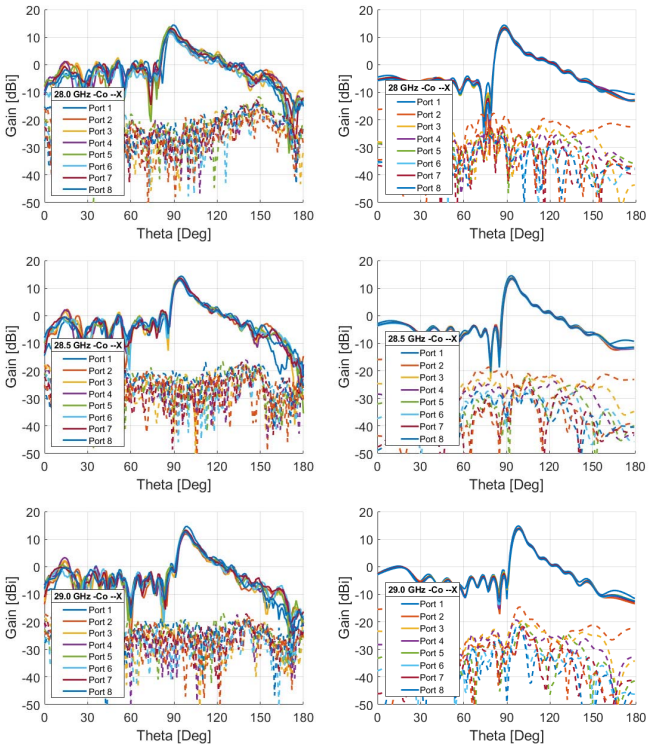

Fig. 15. Vertical cuts of the embedded radiation patterns at 28, 28.5, and 29 GHz. Left: Measured. Right: Simulated.

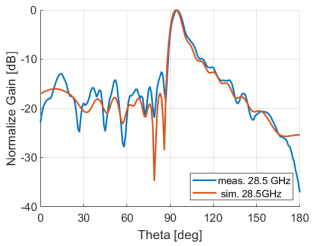

Fig. 16. Comparison of the measured vertical cut with simulation at 28.5 GHz.

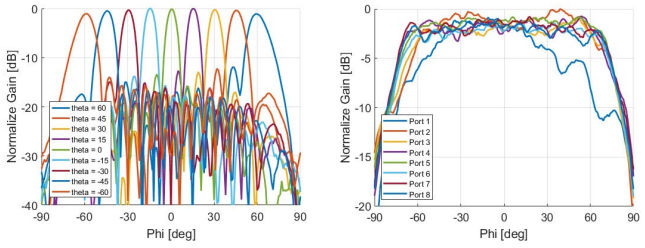

Fig. 17. Scanning performance of the phased array at 28 GHz (left) based on measured embedded radiation patterns (right).

The simulated realized gain of the overall antenna system of sixteen subarrays was 25.7 dBi with the total efficiency of 78%.

The important parameter of the series fed array is beam squint. The design allows for the impedance bandwidth of 4 GHz. Naturally, the overall beam squint over such wide frequency band is large. Nevertheless, depending on the local spectral regulations, only part of this band will be used to transmit 5G signals with total simultaneous bandwidth of 400 MHz. The beam squint is 4° in such case and the variation of the power within the beam varies is less than 2.5 dB.

The scan radiation patterns at 28 GHz are shown in Fig. 17. A grating-lobe-free beam scanning range of up to ±60° is achieved. The maximum level of the sidelobes is below −12 dB in the whole scanning range. Further reduction in the SLL can be achieved by dedicated amplitude or space tapering. The gain variation due to scan loss is only ±0.5 dB. It is due to the wide embedded patterns which have beamwidth of 150° [see Fig. 17 (right)] and the low MC between the subarrays.

V. Comparison of Cosecant-Squared Array With Traditional Patch Array

Most of the proposed array topologies consist of square 8 × 8 or 16 × 16 arrays of microstrip patches with square lattices and half-wavelength element spacing. Such designs are not optimally suited for 5G base station antennas typically placed on pole and looking down, because, as we prove in [5], around 98% of ground level users are normally within an angle of 20° from the light pole horizon. Other drawbacks of the traditional arrays are in their massive complexity, power consumption, and heat generation, particularly if full digital beam forming is used.

The main advantages of cosecant-squared approach are:

1) Simplicity and low cost.
2) *Digital Beamforming With Limited Complexity:* The DBF complexity is directly related to the number of elements (or subarrays) used in the system. If we assume a fast, reliable, and low-complexity precoding via simple beam steering, the number of mathematical operations that should be performed is proportional to $(14 \times N - 2)$ [38] where N is the total number of control points. In the 16 × 16 array, N is equal to 256, while in the array of cosecant subarrays, N is equal to 16. The reduction in the processing complexity will be much more significant if a more complex precoding algorithm, such as zero-forcing, is used for which the required number of operations is proportional to higher orders of N [38].
3) *Received Power Equalization at All Distances With High Electronics Efficiency:* The cosecant-squared shape adjusts the transmit antenna gain so that the users (with similar height) receive the same power, independent of their distance to the base station. Thus, adaptive power transmission to prevent overshadowing is not needed and all the power amplifiers (PAs) can work efficiently at optimal power level.
4) *Easy Cooling:* In an array of cosecant subarrays, all the chips are located on one side of the board. Therefore, the integration of a cooling system (heat pipes, cold plates, and so on) is easier. Moreover, the heat can be quickly transferred to the array side where an additional cooling system can be placed [39].

TABLE IV
COMPARISON OF COSECANT-SQUARED ARRAY WITH TRADITIONAL PATCH ARRAYS

Parameters	Cosecant approach	8×8 patch array	16×16 patch array
Gain of sub-array or patch	15 dBi	6 dBi	6 dBi
EIRP*	57.1 dBm	60.1 dBm	72.2 dBm
Overall bandwidth**	3.5 %	7-8 %	
Dual-pol realization	Complex	Simple	
Cooling	Passive	Active	
DBF complexity	Low	Medium	High

*assumed maximum output power of 18dBm of the amplifier behind each element/sub-array.
**overall bandwidth taken in account impedance and radiation bandwidth.

There are also some drawbacks coming with cosecant-shaped approach and its realization with SIW technology.

1) *Relatively Large Input Power to Each Port:* If the same chips are used in the 2-D array and the cosecant-squared subarray, there will be much less power in the cosecant-squared array due to the reduced number of chips, thus much less EIRP which limits the cell range. Therefore, larger PAs are needed in the array of cosecant subarrays.
2) *Single Polarization:* We realize the cosecant-squared subarray with vertical polarization in SIW technology. It makes the design of the dual-pol antenna system more complex. Practically, it would mean to use relatively high permittivity laminates to be able to put SIW feeding lines for both polarization close to each other and realize the scanning range $+/-60°$.
3) *Poor Radiation Bandwidth:* The antenna array exhibits impedance bandwidth of 18%; however, the radiation bandwidth is about 3.5%. It is due to the realization of the cosecant-squared shaped pattern by the series-fed antenna array with feeding at one end. It causes the beam squint of about $\pm 4°$ in frequency band of 1 GHz. The radiation bandwidth can be improved with the feeding in center of the antenna array.

Table IV summarizes general comparison of the cosecant-squared array with traditional patch arrays.

VI. CONCLUSION

In this article, a novel concept of millimeter-wave antenna array for the 5G base stations is proposed. To satisfy challenging requirements of 5G applications in terms of multibeam generation capability with large scanning area and low-cost implementation, an SIW-based phased array antenna with cosecant-squared shaped radiation pattern in the elevation plane is proposed. To achieve high-gain radiation patterns in the elevation plane and wideband impedance matching, a novel radiating element consisting of a transversal slot in SIW and aperture coupled patch with two tuning components (vertical vias and phase element) has been proposed and designed for particular application. The antenna array exhibits impedance bandwidth of 18% and consistent cosecant-squared radiation patterns in a frequency band of 3.5% (bandwidth reduction in comparison with the impedance is due to beam squint). This is considerable improvement over the basic element slot from [24] with the gain of about 5.5 dBi and the operational bandwidth of the subarray was about 1%. The azimuth scanning range of the phased array with low scan loss is more than $+/-60°$. The array design has been experimentally verified by manufacturing of the array and measuring its impedance properties and radiation patterns. The array concept proposed has clear advantages of typical 5G square arrays in terms of complexity, required RF, and computational power and cooling.

ACKNOWLEDGMENT

The authors would like to thank Pascal Aubry for his help in measurements of the manufactured antenna array.

REFERENCES

[1] *IEEE International Network Generations Roadmap*, 1st ed. Hardware Roadmap, Chennai, India, 2019.
[2] W. Hong *et al.*, "Multibeam antenna technologies for 5G wireless communications," *IEEE Trans. Antennas Propag.*, vol. 65, no. 12, pp. 6231–6249, Dec. 2017.
[3] Y. Aslan, J. Puskely, A. Roederer, and A. Yarovoy, "Active multiport subarrays for 5G communications," in *Proc. IEEE-APS Topical Conf. Antennas Propag. Wireless Commun. (APWC)*, Sep. 2019, pp. 298–303.
[4] Y. Aslan, J. Puskely, A. Roederer, and A. Yarovoy, "Trade-offs between the quality of service, computational cost and cooling complexity in interference-dominated multi-user SDMA systems," *IET Commun.*, vol. 14, no. 1, pp. 144–151, Jan. 2020.
[5] Y. Aslan, S. Salman, J. Puskely, A. Roederer, and A. Yarovoy, "5G multi-user system simulations in line-of-sight with space-tapered cellular BaseStation phased arrays," in *Proc. 13th EuCAP*, Krakow, Poland, Apr. 2019, pp. 1–5.
[6] R. J. Mailloux, *Phased Array Antenna Handbook*. Norwood, MA, USA: Artech House, 2005.
[7] I. Ahmed *et al.*, "A survey on hybrid beamforming techniques in 5G: Architecture and system model perspectives," *IEEE Commun. Surveys Tuts.*, vol. 20, no. 4, pp. 3060–3097, 4th Quart., 2018.
[8] A. F. Molisch *et al.*, "Hybrid beamforming for massive MIMO: A survey," *IEEE Commun. Mag.*, vol. 55, no. 9, pp. 134–141, Sep. 2017.
[9] C. Kyun Ng, M. Ismail, B. M. Ali, S. Khatun, and S. S. Jamuar, "Impact of inter-cell interference on capacity in the joint multiple access (CDMA and SDMA) system," in *Proc. Asia–Pacific Conf. Commun.*, Oct. 2005, pp. 435–439.
[10] T. Kopacz and D. Heberling, "Impact of the elevation scanning angle on the vertical compliance distance of 5G massive MIMO antennas," in *Proc. 13th EuCAP*, Krakow, Poland, Apr. 2019, pp. 1–5.
[11] S. Salman, Y. Aslan, J. Puskely, A. Roederer, and A. Yarovoy, "System modeling and simulation in 5G: A hybrid beamforming approach with power flux equalization in the elevation plane," in *Proc. 49th Eur. Microw. Conf. (EuMC)*, Oct. 2019, pp. 746–749.
[12] A. Dastranj, H. Abiri, and A. Mallahzadeh, "Design of a broadband cosecant squared pattern reflector antenna using IWO algorithm," *IEEE Trans. Antennas Propag.*, vol. 61, no. 7, pp. 3895–3900, Jul. 2013.
[13] M. Milijić, A. D. Nešić, and B. Milovanović, "Design, realization, and measurements of a corner reflector printed antenna array with cosecant squared-shaped beam pattern," *IEEE Antennas Wireless Propag. Lett.*, vol. 15, pp. 421–424, 2015.
[14] E. Carrasco, M. Barba, J. A. Encinar, M. Arrebola, F. Rossi, and A. Freni, "Design, manufacture and test of a low-cost shaped-beam reflectarray using a single layer of varying-sized printed dipoles," *IEEE Trans. Antennas Propag.*, vol. 61, no. 6, pp. 3077–3085, Jun. 2013.

[15] M. Arrebola, J. A. Encinar, and M. Barba, "Multifed printed reflectarray with three simultaneous shaped beams for LMDS central station antenna," *IEEE Trans. Antennas Propag.*, vol. 56, no. 6, pp. 1518–1527, Jun. 2008.
[16] J. Lei, G. Fu, L. Yang, and D.-M. Fu, "Wide band linear printed antenna array with low sidelobe cosecant square-shaped beam pattern," *Prog. Electromagn. Res. C*, vol. 15, pp. 233–241, 2010.
[17] A. Kedar, P. N. S. Kutiyal, M. Garg, and U. K. Revankar, "Wide band low profile linear microstrip antenna array with cosecant square-shaped beam pattern," *Microw. Opt. Technol. Lett.*, vol. 49, no. 4, pp. 963–965, 2007.
[18] M. Koubeissi, L. Freytag, C. Decroze, and T. Monediere, "Design of a cosecant-squared pattern antenna fed by a new butler matrix topology for base station at 42 GHz," *IEEE Antennas Wireless Propag. Lett.*, vol. 7, pp. 354–357, 2008.
[19] Z.-C. Hao and M. He, "Developing millimeter-wave planar antenna with a cosecant squared pattern," *IEEE Trans. Antennas Propag.*, vol. 65, no. 10, pp. 5565–5570, Oct. 2017.
[20] H. Chu, P. Li, and Y.-X. Guo, "A beam-shaping feeding network in series configuration for antenna array with cosecant-square pattern and low sidelobes," *IEEE Antennas Wireless Propag. Lett.*, vol. 18, no. 4, pp. 742–746, Apr. 2019.
[21] J. Hirokawa, C. Yamazaki, and M. Ando, "Postwall waveguide slot array with cosecant radiation pattern and null filling for base station antennas in local multidistributed systems," *Radio Sci.*, vol. 37, no. 2, pp. VIC10-1–VIC10-7, Dec. 2002.
[22] S. Yamamoto, J. Hirokawa, and M. Ando, "A beam switching slot array with a 4-way butler matrix installed in a single layer post-wall waveguide," in *Proc. IEEE Antennas Propag. Soc. Int. Symp.*, Jun. 2002, pp. 138–141.
[23] C. Sacchi, T. F. Rahman, N. Bartolomei, S. Morosi, A. Mazzinghi, and F. Ciabini, "Design and assessment of a CE-OFDM-based mm-wave 5G communication system," in *Proc. IEEE Globecom Workshops (GC Wkshps)*, Dec. 2016, pp. 1–7.
[24] T. Mikulasek, J. Puskely, A. G. Yarovoy, J. Lacik, and H. Arthaber, "Transverse slot with control of amplitude and phase for travelling-wave SIW antenna arrays," *IET Microw., Antennas Propag.*, vol. 14, no. 15, pp. 1943–1946, Dec. 2020.
[25] J. Puskely, Y. Aslan, A. Roederer, and A. Yarovoy, "SIW based antenna array with power equalization in elevation plane for 5G base stations," in *Proc. 12th Eur. Conf. Antennas Propag. (EuCAP)*, Apr. 2018, pp. 5–65.
[26] L. Yan, W. Hong, K. Wu, and T. J. Cui, "Investigations on the propagation characteristics of the substrate integrated waveguide based on the method of lines," *IEE Proc. Microw. Antennas Propag.*, vol. 152, no. 1, pp. 35–42, Feb. 2005.
[27] O. M. Bucci, G. Franceschetti, G. Mazzarella, and G. Panariello, "A general projection approach to array synthesis," in *Dig. Antennas Propag. Soc. Int. Symp.*, Jun. 1989, pp. 146–149.
[28] B. Fuchs, "Synthesis of sparse arrays with focused or shaped beampattern via sequential convex optimizations," *IEEE Trans. Antennas Propag.*, vol. 60, no. 7, pp. 3499–3503, Jul. 2012.
[29] N. V. S. N. Sarma and R. Chandrasekharam, "Shaped beam radiation pattern synthesis using genetic algorithm," in *Proc. IEEE ICEMIC*, Hyderabad, India, Dec. 1999, pp. 171–174.
[30] A. K. Behera, A. Ahmad, S. K. Mandal, G. K. Mahanti, and R. Ghatak, "Synthesis of cosecant squared pattern in linear antenna arrays using differential evolution," in *Proc. IEEE Conf. Inf. Commun. Technol.*, Apr. 2013, pp. 1025–1028.
[31] X.-M. Zhang, K. M. Luk, Q.-F. Wu, T. Ying, X. Bai, and L. Pu, "Cosecant-square pattern synthesis with particle swarm optimization for nonuniformly spaced linear array antennas," in *Proc. 8th Int. Symp. Antennas, Propag. EM Theory*, Nov. 2008, pp. 193–196.
[32] A. Akdagli and K. Guney, "Shaped-beam pattern synthesis of equally and unequally spaced linear antenna arrays using a modified tabu search algorithm," *Microw. Opt. Technol. Lett.*, vol. 36, no. 1, pp. 16–20, Jan. 2003.
[33] W. Stutzman, "Synthesis of shaped-beam radiation patterns using the iterative sampling method," *IEEE Trans. Antennas Propag.*, vol. AP 19, no. 1, pp. 36–41, Jan. 971.
[34] Y. Aslan, J. Puskely, A. Roederer, and A. Yarovoy, "Performance comparison of single- and multi-lobe antenna arrays in 5G urban outdoor environmentsat mm-Waves via intelligent ray tracing," in *Proc. 14th EuCAP*, Copenhagen, Denmark, Mar. 2020, pp. 1–5.
[35] Y. Aslan, J. Puskely, A. Roederer, and A. Yarovoy, "Synthesis of multiple beam linear arrays with uniform amplitudes," in *Proc. 12th Eur. Conf. Antennas Propag. (EuCAP)*, Apr. 2018, pp. 5–65.
[36] Y. Aslan, J. Puskely, A. Roederer, and A. Yarovoy, "Phase-only control of peak sidelobe level and pattern nulls using iterative phase perturbations," *IEEE Antennas Wireless Propag. Lett.*, vol. 18, no. 10, pp. 2081–2085, Oct. 2019.
[37] D. Gies and Y. Rahmat-Samii, "Particle swarm optimization for reconfigurable phase-differentiated array design," *Microw. Opt. Technol. Lett.*, vol. 38, no. 3, pp. 172–175, Aug. 2003.
[38] C.-S. Park, Y.-S. Byun, A. M. Bokiye, and Y.-H. Lee, "Complexity reduced zero-forcing beamforming in massive MIMO systems," in *Proc. Inf. Theory Appl. Workshop (ITA)*, Feb. 2014, pp. 1–5.
[39] B. J. Döring, "Cooling system for a Ka band transmit antenna array," German Aerosp. Center (DLR), Köln, Germany, Tech. Rep. IB554-06/02, Dec. 2005.

Jan Puskely was born in Prerov, Czech Republic, in 1982. He received the master's and Ph.D. degrees in electrical engineering from the Brno University of Technology (BUT), Brno, Czechia, in 2007 and 2010, respectively.

He worked as a Post-Doctoral Researcher with the Department of Radioelectronics, Brno University of Technology. He is a Researcher at the Microwave Sensing, Signals and Systems (MS3) Department, Delft University of Technology, Delft, The Netherlands, and at the Netherlands Organization for Applied Scientific Research (TNO), The Hague, The Netherlands. His current research interests include the phased antenna arrays, active and reconfigurable antenna systems, antenna array topologies, and antenna front-end designs at millimeter waves.

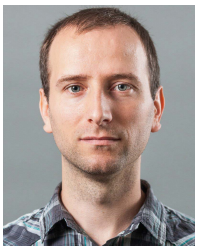

Tomas Mikulasek received the M.Sc. and Ph.D. degrees in electrical engineering and communication from the Brno University of Technology, Brno, Czech Republic, in 2009 and 2013, respectively.

He is currently a Researcher at the Department of Radio Electronics, Faculty of Electrical Engineering and Communication, Brno University of Technology. His research interests include microwave antennas and components based on substrate integrated waveguide (WG) technology.

Yanki Aslan (Member, IEEE) was born in Ankara, Turkey, in 1991. He received the B.Sc. degree, with double specialization in communications and microwaves and antennas, from the Department of Electrical and Electronic Engineering, Middle East Technical University, Ankara, in 2014, and the M.Sc. and Ph.D. degrees *(cum laude)* in electrical engineering from the Delft University of Technology, Delft, The Netherlands, in 2016 and 2020, respectively.

He is currently working as a Post-Doctoral Researcher at Microwave Sensing, Signals and Systems (MS3) Group, Delft University of Technology. His current research interests include phased arrays for next-generation communication and sensing systems, array optimization, multibeam antennas, front-end architectures, and beamforming algorithms.

Dr. Aslan was one of the recipients of the IEEE AP-S Doctoral Research Grant in 2018 and the EuMA Internship Award in 2019. He received the Justus and Louise van Effen Scholarship from the Delft University of Technology for his M.Sc. degree.

Antoine Roederer (Life Fellow, IEEE) was born in Paris, France, in 1943. He received the B.S.E.E. degree from the l'Ecole Superieure d'Electricite, Paris, in 1964, the M.S.E.E. degree from the University of California at Berkeley, Berkeley, CA, USA, in 1965, the Ph.D. degree (Hons.) in electrical engineering from the Universite de Paris VI, Paris, in 1972, and the Honorary Ph.D. degree from the Technical University of Delft, Delft, The Netherlands, in 2005.

He was a Radar Antenna Research and Development Engineer with THOMSON-CSF, Bagneux, France, from 1968 to 1973. He joined the European Space Research and Technology Centre, ESRO (now ESA, the European Space Agency), Noordwjik, The Netherlands, in 1973, where he initiated and supervised for many years research and development and project support for space antennas. In 1993, he became the Head of the Electromagnetics Division, ESA, where he retired in 2008. He is currently a part-time Scientific Advisor with the Technical University of Delft. He has authored or coauthored over 150 articles, several book chapters, and holds 20 patents in the field of antennas. This has included aspects of wideband communications, broadcasting, radar, and satellite antennas, with an emphasis on log-periodics, reflectarrays, multiple-beam reflectors and arrays, and advanced antenna feed networks. His current research interests include innovation and development in the fields of radar and 5G base station antennas.

Dr. Roederer received numerous awards for his contributions to the field of antennas and to the antenna community in Europe. He received the Fulbright Fellowship for his M.S.E.E. degree. He has been the Chairman of the EU COST 260 Project on Smart Antennas. He was the Initiator and the Chairman of the Millennium Conference on Antennas and Propagation (AP 2000), Davos, precursor of the large EUCAP conferences.

Alexander Yarovoy (Fellow, IEEE) received the Diploma degree (Hons.) in radiophysics and electronics and the Candidate Phys. and Math.Sci. and Doctor Phys. and Math.Sci. degrees in radiophysics from Kharkov State University, Kharkiv, Ukraine, in 1984, 1987, and 1994, respectively.

In 1987, he joined the Department of Radiophysics, Kharkov State University, as a Researcher, where he became a Professor in 1997. From September 1994 to 1996, he was with the Technical University of Ilmenau, Ilmenau, Germany, as a Visiting Researcher. Since 1999, he has been with the Delft University of Technology, Delft, The Netherlands. Since 2009, he has been leading the Chair of Microwave Sensing, Systems and Signals. He has authored or coauthored more than 450 scientific or technical articles, four patents, and 14 book chapters. His main research interests are in high-resolution radar, microwave imaging, and applied electromagnetics (in particular, UWB antennas).

Dr. Yarovoy was a recipient of the European Microwave Week Radar Award for the paper that best advances the state of the art in radar technology in 2001 (together with L. P. Ligthart and P. van Genderen) and in 2012 (together with T. Savelyev). In 2010, together with D. Caratelli, he received the Best Paper Award from the Applied Computational Electromagnetic Society (ACES). He served as the General TPC Chair of the 2020 European Microwave Week (EuMW'20), the Chair and the TPC Chair of the Fifth European Radar Conference (EuRAD'08), and the Secretary of the First European Radar Conference (EuRAD'04). He also served as the Co-Chair and the TPC Chair of the Xth International Conference on GPR (GPR2004). He served as a Guest Editor for five special issues of the IEEE Transactions and other journals. Since 2011, he has been an Associate Editor of the *International Journal of Microwave and Wireless Technologies*. From 2008 to 2017, he served as the Director for the European Microwave Association (EuMA).